THE JOURNAL OF PHYSICAL CHEMISTRY A

Article

pubs.acs.org/JPCA

Pyrrolyl−Silicon Compounds as Precursors for Donor−Acceptor Systems Stabilized by Noncovalent Interactions

Susana González-Santana,[§] Cercis Morera-Boado,[§] Luis A. Montero-Cabrera,[§] Monica Trueba,*[,#] and Stefano P. Trasatti[#]

[§]Department of Physical Chemistry, Faculty of Chemistry, Universidad de la Habana, Zapata y G, 10400 Ciudad de La Habana, Cuba
[#]Department of Chemistry, Università degli Studi di Milano, Via Golgi 19, 20133 Milan, Italy

Supporting Information

ABSTRACT: Pyrrolyl−silicon compounds were investigated by different theoretical approaches. Model monomers consisted of a pyrrole ring N-substituted with silylmethoxy and silylhydroxy end groups through a propyl chain spacer, designated as PySi and PySiOH. Geometrical, vibrational, and electronic properties, as well as chemical reactivity, are discussed and compared with pyrrole (Py) and *N*-propylpyrrole (*N*-PrPy) that were studied in parallel for reference purposes and methods validation. The electronic distribution between PySi and PySiOH differs importantly, the former being an electron donor, as Py and *N*-PrPy. Conversely, PySiOH presents donor−acceptor character with the LUMO energy level localized on the silanol end group. Global and local reactivity descriptors predict PySiOH more reactive than PySi with two preferential reactive sites: electron-rich Py ring and electron-deficient silanol group. On the basis of experimental studies, oligomers of PySiOH linked $\alpha-\alpha'$ via Py rings ($\alpha-\alpha'Py_nSiOH$, n = 2, 3) were considered as model molecules of hydrolyzed PySi. The most stable structures were derived from randomly generated $\alpha-\alpha'Py_nSiOH$ that were optimized at semiempirical AM1 and refined with M05-2X/6-31G(d,p). Conformational analysis of dimer and trimer structures points to stability enhanced by molecular packing. Nonetheless, NBO and RDG results indicate that oligomer stability is dictated by the cooperative contribution of hydrogen bonding between silanol end groups and dispersive vdW interactions between silanol and the π system of the Py ring. The latter interaction resulting from electron delocalization induced by an electron-deficient silanol group seems to determine the smaller gap energy of T-shaped OH−π arrangements. The theoretical findings support the peculiar chemical behavior revealed by experiment.

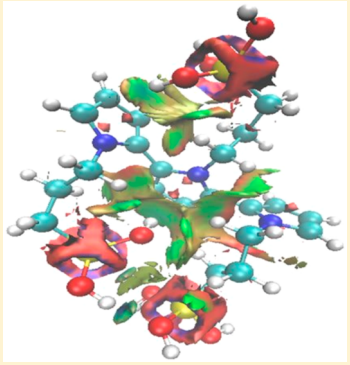

1. INTRODUCTION

A practical problem concerning the structure of pyrrole agglomerates in solutions of *N*-[3-(trimethoxysilyl)propyl]-pyrrole (PySi) (Figure 1a) has motivated this theoretical study. Just for introducing it, silanes functionalized with pyrrole and aniline have been extensively used by some of the coauthors for surface treatment of Al alloys to provide corrosion protection.[1−7] The surface treatment consists of the immersion of metallic specimens in the corresponding silane hydrolyzed solution for some time and subsequent thermal treatment at relatively low temperatures. Silanol intermediates coordinate with the OH-rich metal surface through hydrogen bonding. Heating promotes water elimination and covalent oxane bonds at the metal/film interface (Me−O-Si), as well as within the adsorbed layer (Si−O−Si). The resulting hybrid films are typically thin (2−5 μm), compact, and well-adhered. The very good corrosion protection is related to the barrier action provided by the siloxane network, which limits aggressive species penetration toward the metal/film interface, and pyrrole (or aniline) moieties that act on demand to keep the metal passive in small defects as siloxane linkage fails. From combined spectroscopic characterization of treated surfaces and of hydrolyzed solutions, the protection capacity of the hybrid film is importantly influenced by pyrrole (or aniline) agglomerates. The active protection seems to be enhanced by the semiconducting properties of the hybrid films.[6,7] Although the reactivity of pyrrole and aniline units increases by promoting hydrolysis, only for PySi is the condensation of silanol groups limited with time. Some relevant results of PySi solutions obtained by means of attenuated total reflection IR (ATR-IR), NMR (^{1}H, ^{13}C, ^{29}Si), and UV−vis spectroscopies are summarized by the end of this paper. Moreover, the corresponding hybrid film (deposited on FTO substrate) presents n-type semiconductor behavior, differently from aniline-based silane (p-type semiconductivity), as obtained recently by photocurrent spectroscopy.[7] It is difficult to rationalize the structure of soluble oligomers favoring the kinetic stabilization of silanol and how they assemble in the macromolecular network.

It is well-known that the silanol group is an important intermediate not only in interfacial adsorption behavior[8] but also in many chemical processes.[9] Most organosilanols form hydrogen-bonded complexes with themselves, water, and

Received: April 30, 2015
Published: June 11, 2015

DOI: 10.1021/acs.jpca.5b04167
J. Phys. Chem. A 2015, 119, 7038−7051

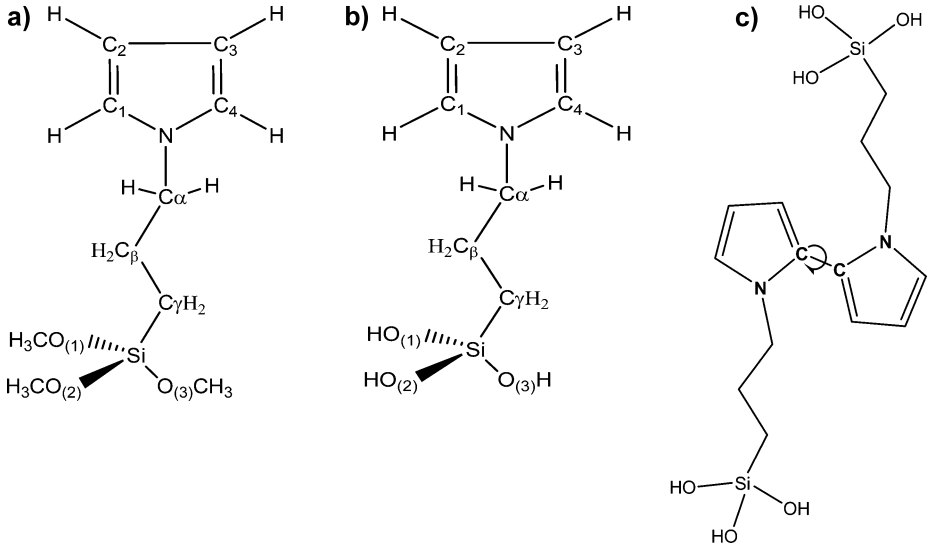

Figure 1. Schematic structures of (a) *N*-[3-(trimethoxysilyl)propyl]pyrrole (PySi), (b) *N*-[3-(trihydroxysilyl)propyl]pyrrole (PySiOH), and (c) PySiOH oligomers linked $\alpha-\alpha'$ via pyrrole rings Py_nSiOH (n = 2, 3). The arrow indicates the inter-ring NCCN rotational angle (θ). The atoms labels in (a, b) denote those used for validation of the monomer geometries (Supporting Information, Tables S1 and S2).

solvent molecules prior to condensation. Electron-deficienct aromaticity has been predicted for silicon nanoclusters, where overcoordinated silicon induces electron delocalization and thus enhanced stability.[10] Monomers such as pyrrole and derivatives are important building blocks in naturally occurring processes and in synthetic materials.[11−13] Monomer reactivity is influenced markedly by steric and electronic properties of the substituents.[14−18] Experimental and/or theoretical studies of pyrrole functionalized with silicon-based groups are few.[19−22]

All above have prompted us to theoretically investigate molecular properties of PySi (Figure 1a) and fully hydrolyzed PySi, namely *N*-[3-(trihydroxysilyl)propyl]pyrrole (PySiOH) (Figure 1b), as well as PySiOH oligomers linked $\alpha-\alpha'$ via pyrrole rings ($\alpha-\alpha'Py_nSiOH$, n = 2, 3) (Figure 1c). Ground-state geometries of model monomers were optimized at different semiempirical and DFT levels of theory. For reference purposes and theoretical methods validation, pyrrole (Py) and *N*-propylpyrrole (*N*-PrPy) were investigated also. Monomer reactivity was estimated by conceptual DFT through global reactivity descriptors and local (condensed) Fukui functions. Reported studies have indicated good correlation between these functions and experimental electrophilic substitution patterns for a range of aromatic heterocyclic compounds,[23−29] including pyrrole derivatives[27] and silicon-based materials.[28,29] Multiple minima hypersurface (MMH) methodology, the validity of which for the study of molecular associations and for conformational analysis has been widely demonstrated by some of the coauthors,[30−38] was employed for random generation and optimization at semiempirical level of theory of $\alpha-\alpha'Py_nSiOH$ (n = 2, 3). Most stable structures were DFT-refined for conformational analysis. Noncovalent stabilizing interactions were estimated by means of natural bond orbital (NBO) and reduced density gradient (RDG) analyses. Conclusions are drawn by considering computational results and experimental data.

2. THEORETICAL METHODS AND COMPUTATIONAL DETAILS

Equilibrium geometries of Py, *N*-PrPy, PySi, and PySiOH were calculated using semiempirical AM1[39] and PM3[40] Hamiltonians with the MOPAC 2009 program.[41] Optimized structures at higher levels of theory were obtained with DFT functional methods B3LYP[42] and M05-2X[43,44] with the 6-31G(d,p) basis set, as implemented in Gaussian09.[45] For each theoretical method, the mean deviation (MD) of the difference between theoretical (X_i) and experimental (X_{exp}) internal coordinates (bonds and angles) was calculated with the equation

$$\mathrm{MD} = \frac{\sum_N^{i=1} |X_i - X_{\mathrm{exp}}|}{N}$$

The chemical reactivity and site selectivity were estimated by conceptual DFT.[23] Global reactivity descriptors such as electronegativity (χ), chemical potential (μ), hardness (η), softness (S), and electrophilicity index (ω), were calculated using HOMO and LUMO energies of frontier molecular orbitals with equations

$$\chi = -1/2(\varepsilon_{\mathrm{LUMO}} + \varepsilon_{\mathrm{HOMO}})$$

$$\mu = -\chi = 1/2(\varepsilon_{\mathrm{LUMO}} + \varepsilon_{\mathrm{HOMO}})$$

$$\eta = 1/2(\varepsilon_{\mathrm{LUMO}} - \varepsilon_{\mathrm{HOMO}})$$

$$S = 1/\eta$$

$$\omega = \mu^2/2\eta$$

CM5PAC package[46−48] was used for Charge Model 5 (CM5) partial atomic charges calculation using Hirshfeld atomic charges from Gaussian09 output files. Then, local (condensed) Fukui functions f_k^- and f_k^+, for electrophilic and nucleophilic attack, respectively, were estimated at M05-2X/6-31G(d,p) with the following equations:

$$f_k^- = q_k(N) - q_k(N-1)$$

$$f_k^+ = q_k(N+1) - q_k(N)$$

where q_k represents the atomic charge at the kth atomic site, according to the Hirshfeld partitioning scheme for electron density distribution among the atoms. The terms (N), ($N+1$), and ($N-1$) correspond to the electron populations on atom k

DOI: 10.1021/acs.jpca.5b04167
J. Phys. Chem. A 2015, 119, 7038−7051

present in neutral, anion, and cation states of the molecule, respectively.[23]

Multiple minima hypersurface (MMH) methodology was used for random generation of 500 configurations of $\alpha-\alpha'$Py$_n$SiOH dimer (n = 2) and trimer (n = 3) structures, allowing free rotation of inter-ring torsion angles ∠NCCN (θ), with the help of GRANADAROT program,[49] and subsequent optimization at semiempirical the AM1 level of theory. A representative number of stable oligomer conformations in each set of dimer and trimer structures were submitted to single-point energy DFT calculations using M05-2X/6-31G-(d,p). The nature of the stationary points (i.e., true minima or transition state) was determined by vibrational frequency calculations. The most stable ground-state configurations of $\alpha-\alpha'$ Py$_n$SiOH oligomers at the M05-2X/6-31G(d,p) level were selected for conformational analysis. The second-order perturbation theory was applied through NBO calculations[50,51] to estimate the energetic importance on oligomers stability of all the possible interactions between filled donor and empty acceptor NBOs, as well as charge transfer between Lewis and non-Lewis type orbitals. The reduced density gradient (RDG) function, defined as RDG = $c_s|\nabla\rho|/\rho^{4/3}$), where c_s is the inverse of the Fermi constant $(1/2(3\pi^2)^{1/3})$, was calculated to distinguish weak interaction regions such as van der Waals (vdW) and hydrogen bonding.[52−54] The real space function sign($\lambda_{2(r)}$) $\rho(r)$, defined by the product of the sign of the second eigenvalue of the Hessian λ_2 by the density $\rho(r)$, was used to fill RDG surfaces with different colors to distinguish the type of interaction.

3. RESULTS AND DISCUSSION

3.1. Monomers. Ground-state geometries of PySi and PySiOH (Figure 1a,b), as well as of Py and *N*-PrPy (not shown) were calculated using different theoretical methods. Calculated bond distances and angles at different levels of theory, namely semiempirical AM1 and PM3, and DFT M05-2X and B3LYP with 6-31G(d,p) basis set, reported experimental values,[26,55−65] and mean deviations (MD), are supplied as Supporting Information (Tables S1 and S2). Figure 2 shows graphically MD values of bond distances (top) and angles (bottom) for each method of calculation. Very good agreement with experiment is obtained for bond distances with DFT functionals M05-2X/6-31G(d,p) and B3LYP/6-31G(d,p). Among the semiempirical methods, PM3 predicts better the bond length, whereas AM1 underestimate Cγ-Si for PySi and PySiOH (Table S1, Supporting Information).

For bond angles (Figure 2, bottom), MD values are higher but change little with the quality of calculation, though AM1 and M05-2X/6-31G(d,p) likely estimate better this geometrical coordinate. B3LYP/6-31G(d,p) overestimates Si−O−C angles by 5° for PySi monomer (Table S2, Supporting Information). Regardless of the level of theory, the internal angles of Py ring were between 107 and 110° for all the monomers, indicating small distortion of Py ring from C_{2v} symmetry with N-substitution. Similarly, the dihedral angles ∠NC$_\alpha$C$_\beta$C$_\gamma$ and ∠C$_\alpha$C$_\beta$C$_\gamma$Si of the corresponding N-side chains were between 178 and 180°, indicating all-*trans* configuration.

Theoretical vibrational analysis (Table S3, Supporting Information) showed vibrations associated with the functional groups of the side chain and to interactions between component functional groups and/or basic substructure of N-substituted monomers, in addition to the 24 fundamentals of Py ring. From comparison of theoretical results with

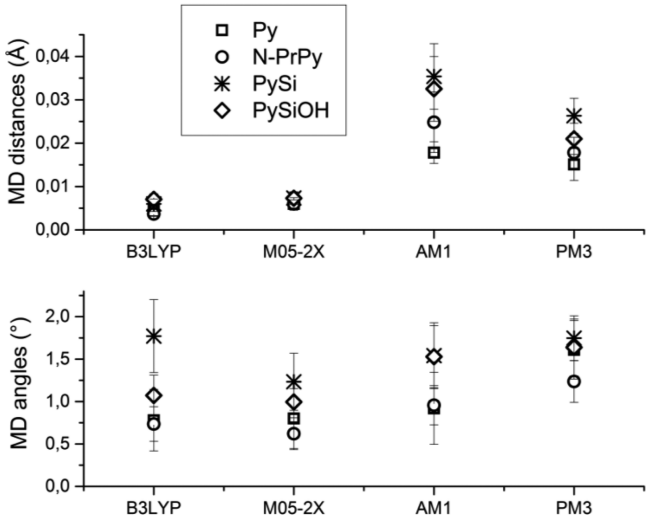

Figure 2. Mean deviation (MD) of internal coordinates, bond distances (top) and bond angles (bottom), of the monomers Py, PrPy, PySi, and PySiOH, calculated with AM1 and PM3 semiempirical hamiltonians and density functional methods B3LYP and M05-2X with basis set 6-31G(d,p). Error bars correspond to the standard deviation.

experimental data for Py in the gas phase,[66−69] the root-mean-square (rms) deviation of 25.0 cm^{-1} is in the range of reported rms values using other theoretical methods with double-ζ 6-31G basis sets (17.4−43.9 cm^{-1}).[64] Good agreement with experiment is indicated also for *N*-PrPy by considering the experimental IR data of *N*-butylpyrrole neat liquid,[70] with the exception of CH$_3$ stretching vibrations and C−C scissoring of the propyl chain that are shifted to higher frequencies by 40−50 cm^{-1} for the former. The theoretical vibrations of PySi and PySiOH (Table S3, Supporting Information) were compared with experimental ATR-IR spectra of PySi neat liquid and of its hydrolyzed methanol-based solution (after solvent evaporation),[1] as well as with experimental IR data for neat liquid of *N*-[(triethoxysilyl)-methyl]pyrrole[14] and IR/Raman for triethylsilanol (gas phase and neat liquid).[71] The agreement between theory and experiment is quite satisfactory, with the exception of SiOH vibrations for PySiOH and PySi hydrolyzed solution due to hydrogen bonding and siloxane linkages promoted in the latter (broad bands between 3600−3100, 1100−1050, and 900−800 cm^{-1}).[1] Nonetheless, theoretical stretching vibrations of free OH groups ν_{OH} ≅ 3720−3728 cm^{-1} are in very good agreement with experimental gas phase data of triethylsilanol (3730 cm^{-1})[71] (Table S3, Supporting Information). From comparison of theoretical Py ring fundamentals, major differences are obtained for B2ν_{20-22}, A1$\nu_{4,5}$, A1ν_8, and A1ν_9. With N-substitution, the frequency and intensity of B2ν_{20-22} and A1$\nu_{4,5}$ decrease and increase similarly. Also the intensity of A1ν_8 and A1ν_9 decreases and increases, respectively, but the frequency is higher for *N*-PrPy and PySiOH and smaller for PySi, in comparison to the case for the Py ring. Although these fundamentals are affected mostly by spatial/mechanical interactions (twisting) and motions such as scissoring and wagging of −CH$_2$ groups of the alkyl spacer, PySi presents less symmetric mass center due to the bulky methoxy end groups.

Table 1 reports HOMO and LUMO energy levels (ε_H, ε_L), gap energies ($E_g = \varepsilon_L - \varepsilon_H$), global reactivity descriptors, and global dipole moments, as obtained at M05-2X and B3LYP

DOI: 10.1021/acs.jpca.5b04167
J. Phys. Chem. A 2015, 119, 7038−7051

Table 1. Calculated HOMO and LUMO Energy Levels (ε_{HOMO}, ε_{LUMO}), Gap Energy ($E_g = \varepsilon_L - \varepsilon_H$), Chemical Potential ($\mu$), Electronegativity ($\chi$), Global Hardness ($\eta$), Global Softness ($S$), and Global Electrophilicity Index (ω) for the Monomers Calculated at B3LYP/6-31G(d,p) and M05-2X/6-31G(d,p) Levels of Theory[a]

	Py		PrPy		PySi		PySiOH	
	M05-2X	B3LYP	M05-2X	B3LYP	M05-2X	B3LYP	M05-2X	B3LYP
ε_{HOMO}	−0.2568	−02023	−0.2526	−0.1985	−0.2516	−0.1969	−0.2496	−0.1955
ε_{LUMO}	0.0985	0.0495	0.0952	0.0473	0.0948	0.0478	0.0887	0.0348
E_g (eV)	9.6674	6.8501	9.4647	6.6885	9.4236	6.6591	9.2043	6.2665
$\chi = -\mu$	2.1527	2.0782	2.1417	2.0567	2.1329	2.0289	2.1886	2.1869
η	4.8337	3.4251	4.7324	3.3442	4.7118	3.3296	4.6022	3.1332
S	0.2068	0.2919	0.2113	0.2990	0.2122	0.3003	0.2173	0.3192
ω	0.4794	0.6305	0.4846	0.6324	0.4827	0.6182	0.5204	0.7632
dipole moment (D)	1.9652	1.9019	2.2930	2.1889	2.9730	2.9399	3.8173	3.7623
ΔN_{max}					−0.0030	−0.0122		
ECT					−0.0229	−0.0886		

[a]Units other than Hartree Atomic Unit are indicated in parenthesis.

with the 6-31G(d,p) basis set. M05-2X/6-31G(d,p) importantly overestimates the experimental E_g of the pyrrole monomer (5.97 eV),[72] as well as the theoretical gas phase E_g = 7.44 eV calculated with B3P86-30% method, which has been proposed as more reliable for estimation of gap energies of CPs oligomers.[73] Nonetheless, E_g = 8.03 eV with M05-2X and higher quality 6-31++G(d,p) basis set, this value being higher than the theoretical B3P86-30% by 0.59 eV. Note that the difference between Eg at B3LYP/6-31G(d,p) and at B3P86-30% is the same. Although the former functional is more popular than meta-exchange−correlation functional M05-2X, incomplete cancellation of self-interaction errors is significantly higher.[43,44] In addition, M05-2X performs better for noncovalent interactions like hydrogen bonding, which cannot be ignored for silanol groups. Even so, both functionals qualitatively predict PySiOH more reactive than PySi (Table 1). With N-substitution, E_g and η decrease, while χ, S, and ω increase, but more importantly for PySiOH. Similarly, the global dipole moment increases markedly, indicating higher directionality of molecular polarization due to unequal sharing of electrons. This global property is less influenced than E_g by the method of calculation, and good agreement with experiment is obtained for Py monomer (1.870−1.890 D).[55]

It is to be noticed also that the decrease of E_g with N-substitution is mainly due to the decrease of LUMO (ε_{LUMO}) rather than of HOMO (ε_{HOMO}) energy levels, regardless of the DFT method. This indicates favored delocalization of the conduction band, more importantly for PySiOH. Frontier orbital maps showed both ε_{LUMO} and ε_{HOMO} localized on the Py ring for all the monomers but PySiOH with LUMO localized on the silanol end group (Figure S4, Supporting Information). Accordingly, this monomer presents an electron-rich Py ring and electron-deficient silanol, indicative of donor−acceptor character.[74−76]

A similar indication is obtained from computed local reactivity descriptors, namely local (condensed) Fukui functions (f_k^-, f_k^+), reported in Tables 2 and 3, where the corresponding isovalent surfaces (0.004 electron/bohr^3) of spin electron density are included. Regardless of the nature of the substituent, f_k^- is higher on α, α' and β, β' carbon atoms of Py ring with ε_{HOMO} localized on the double bonds (Table 2), indicating these sites are electronically enriched. Similarly, the electron density is higher on $C_{\alpha,\alpha'}$, this site being more prone to electrophilic attack. Thus, the nucleophilic nature of Py ring is still important in the presence of methoxysilyl and hydroxysilyl end groups (Figure 1a,b).

Table 2. Condensed Fukui Function (f_k^-) Derived from the Hirshfeld Partitioning Scheme and the Corresponding Isovalent Surfaces (0.04 electron/bohr^3) for Minima Energy Structures of the Monomers at the M05-2X/6-31G(d,p) Level of Theory

Atom	Pyrrole	NPrPy	PySi	PySiOH	Isosurfaces
C 1α	0.203	0.190	0.189	0.189	
C 2	0.119	0.111	0.110	0.110	
C 3	0.119	0.111	0.110	0.111	
C 4α	0.203	0.190	0.189	0.189	
N	0.051	0.034	0.034	0.034	
					Py
H 6	0.045	0.065	0.065	0.065	
H 7	0.071	0.055	0.055	0.055	
H 8	0.059	0.055	0.055	0.055	
H 9	0.059	0.065	0.065	0.065	
H 10	0.071	-	-	-	
Cα(H_2)	-	0.009	0.008	0.008	
Hα1	-	0.021	0.019	0.020	
Hα2	-	0.021	0.019	0.020	
					NPrPy
Cβ(H_2)	-	0.005	0.002	0.002	
Hβ1	-	0.005	0.003	0.004	
Hβ2	-	0.005	0.003	0.003	
Cγ(H_2)	-	0.013	0.007	0.007	
Hγ1	-	0.019	0.009	0.009	
Hγ2	-	0.012	0.008	0.009	
Hγ3	-	0.012	-	-	
Si	-		0.006	0.009	
O1	-		0.002	0.0001	
C_O1	-		0.005	-	
					PySi
H	-		0.006	0.008 (H_O1)	
H	-		0.003	-	
H	-		0.007	-	
O2	-		-0.006	0.011	
C_O2	-		0.004	-	
H	-		0.003	0.007(H_O2)	
H	-		0.005	-	
H	-		0.007	-	
O3	-		0.005	0.0007	
C_O3	-		0.001	-	
H	-		-0.004	0.007(H_O3)	
H	-		0.010	-	PySiOH
H	-	-	-0.003	-	

To evaluate possible intermolecular charge transfer between PySi and PySiOH, based on the coexistence of both monomers in PySi solution at early stages of preparation,[1] the electrophilicity-based charge transfer (ECT) was calculated by[77]

$$ECT = (\Delta N_{max})_A - (\Delta N_{max})_B$$

DOI: 10.1021/acs.jpca.5b04167
J. Phys. Chem. A 2015, 119, 7038−7051

Table 3. Condensed Fukui Function (f_k^+) Derived from the Hirshfeld Partitioning Scheme and the Corresponding Isovalent Surfaces (0.04 electron/bohr^3) for Minima Energy Structures of the Monomers at the M05-2X/6-31G(d,p) Level of Theory

Atom	Pyrrole	NPrPy	PySi	PySiOH	Isosurfaces
C 1α	0.167	0.141	0.093	0.044	
C 2	0.103	0.090	0.063	0.038	
C 3	0.103	0.090	0.063	0.037	
C 4α	0.167	0.141	0.093	0.045	
N	0.109	0.073	0.048	0.021	Py
H 6	0.064	0.069	0.045	0.024	
H 7	0.082	0.054	0.038	0.024	
H 8	0.061	0.054	0.038	0.024	
H 9	0.061	0.069	0.045	0.022	
H 10	0.082	-	-	-	
Cα		0.027	0.017	0.012	
Hα1		0.040	0.026	0.015	
Hα2		0.040	0.023	0.014	NPrPy
Cβ		0.013	0.012	0.013	
Hβ1		0.012	0.011	0.015	
Hβ2		0.012	0.013	0.014	
Cγ		0.018	0.012	0.021	
Hγ1		0.024	0.014	0.025	
Hγ2		0.016	0.013	0.024	
Hγ3		0.016			
Si			0.050	0.148	
O1			0.020	0.044	
C_O1			0.028		PySi
H			0.022	0.065 (H_O1)	
H			0.016		
H			0.022		
O2			0.007	0.070	
C_O2			0.025		
H			0.022	0.120(H_O2)	
H			0.021		
H			0.026		
O3			0.014	0.049	
C_O3			0.019		
H			0.013	0.079(H_O3)	PySiOH
H			0.020		
H			0.008		

where maximum electronic charge $\Delta N_{max} = -\mu/\eta$, and *A* and *B* correspond to PySi and PySiOH (and vice versa). As reported in Table 1, negative ECT values are obtained for both DFT levels of theory, predicting a charge flow from PySi (electron donor) to PySiOH (donor–acceptor). Considering the higher reactivity of PySiOH, α–α' linking of Py rings is likely promoted with methoxy group's hydrolysis, as indicated by experiment.

Concerning f_k^+ (Table 3), still larger values are obtained on $C_{\alpha,\alpha'}$ for PySi, as for Py and *N*-PrPy, conversely to PySiOH with the highest value of f_k^+ on the Si atom, corresponding to LUMO localization. Although computation of atom-condensed Fukui functions depends on the approach employed,[78] the theory predicts important changes of electronic distribution from donor to donor–acceptor behaviors by replacing the methoxy group with a hydroxyl, i.e., from PySi to PySiOH. Although the donor strengths of both monomers are quite similar, the acceptor strength of PySiOH markedly increases due to the electron-deficient silanol end group. Thus, hydrolyzed PySi presents two preferential reactive sites prone to electrophilic attack on electron-rich $C_{\alpha,\alpha}$ of Py ring and to nucleophilic attack on electron-deficient silanol group.

3.2. Conformational Analysis of PySiOH Oligomers (α–α'Py$_n$SiOH). Randomly generated structures of α–α'-Py$_n$SiOH (n = 2, 3) (Figure 1c) with no restriction of inter-ring torsion angle ∠NCCN (θ) were optimized at the semiempirical AM1 level of theory, and the most stable configurations were refined with M05-2X/6-31G(d,p). As pointed out before, these methods estimate better bond angles (Figure 2). In addition, PM3 overestimates hydrogen bonding interactions[79] and M05-2X performs better than B3LYP for noncovalent interactions.[43,44] Conformation assignment was based on torsional angle arrangement (Scheme 1), according to IUPAC terminology.[80]

Scheme 1. Conformation Assignment by Considering Torsional Angle (θ) Arrangement, According to IUPAC Terminology

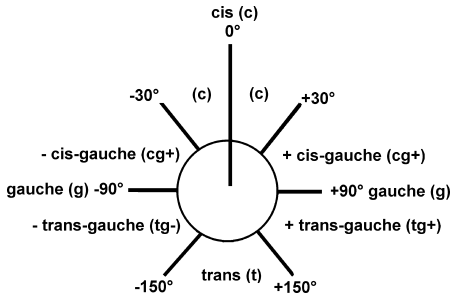

With regard to dimer structures (α–α'Py$_2$SiOH), configurations with θ of 0° (*cis*), 90° (*gauche*), and 180° (*trans*) were not displayed in the MMH output results. Single-point energy calculations at M05-2X/6-31G(d,p) indicated the *trans* conformation as a transition state (one imaginary frequency of 24i cm^{-1}). Thus, only *cis* and *gauche* structures are considered for comparison with M05-2X/6-31G(d,p)//AM1 dimer configurations. Table 4 reports the relative energy (ΔE)

Table 4. Inter-Ring Torsional Angle (θ) and Relative Energy (ΔE) of Py$_2$SiOH Dimer Conformations, As Obtained with M05-2X/6-31G(d,p)

conformation	θ (deg)	ΔE (kcal/mol)
cisv(*c*)	0	23.4
	−20	20.6
cis–*gauche*+ (*cg*+)	41	14.3
	60	11.5
cis–*gauche*– (*cg*–)	−79	8.4
gauche (*g*)	90	5.8
trans–*gauche*+ (*tg*+)	108	6.6
	150	12.9
trans (*t*)	160	14.5
trans–*gauche*– (*tg*–)	−150	3.8
	−121	0
	−94	2.7

and ∠NCCN (θ) of DFT-refined Py$_2$SiOH dimer structures with ΔE < 25 kcal/mol. The plot of ΔE as a function of θ shows no global minimum but two potential energy wells that are energetically nonequivalent (Figure 3). The well with ΔE < 5 kcal/mol is defined by *tg*– configurations, and the second well by conformers with θ > 40°, in particular by *tg*+ (180°) and *g* (90°) with ΔE < 7 kcal/mol. The corresponding optimized geometries are illustrated in Figure 4.

For the analysis of the alkyl side-chain conformation, *trans* and *gauche* orientations correspond to dihedral angles ∠NC$_\alpha$C$_\beta$C$_\gamma$ (τ, τ') and ∠C$_\alpha$C$_\beta$C$_\gamma$Si (ν, ν') outside ±120° and within ±120°, respectively, according to IUPAC

DOI: 10.1021/acs.jpca.5b04167
J. Phys. Chem. A 2015, 119, 7038–7051

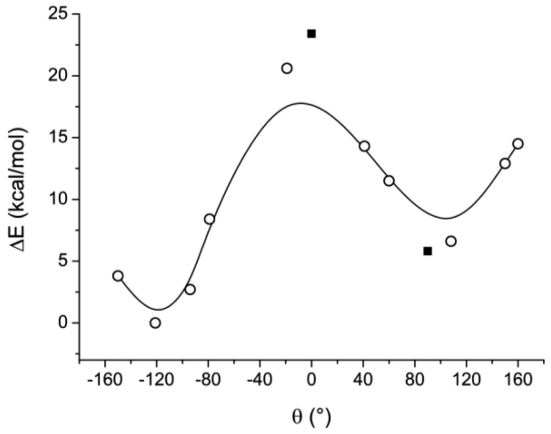

Figure 3. Potential energy curve as a function of inter-ring torsion angle (θ) for $\alpha-\alpha'Py_2SiOH$ conformers at the M05-2X/6-31G(d,p) level of theory: (○) MMH-derived refined structures; (■) optimized structures with fixed θ.

terminology for alkyl chains.[80] When τ, ν and τ', ν' values of the adjacent side chains are plotted as a function of θ (Figure 5), τ and τ' change markedly between ±180° ($t\pm$) and ±75° ($g\pm$). Conversely, $\nu \cong \nu' \cong -75°$ for most conformations, indicating $g-$ preferential space arrangement of silanol-terminated alkyl chain. For most stable $tg-$ dimer structures (ΔE < 5 kcal/mol), $t-g-/g+g-$ orientation prevails for θ = −150° and −121°, whereas $t-g+/t+g-$ for θ = −94°. This dimer as being closer in relative energy to the minima structure (θ = −121°) was confirmed by single-point calculations using M05-2X with the higher quality 6-31++G(d,p) basis set. ΔE decreases from 2.7 to 1.5 kcal/mol, but it does not change for the $tg-$ conformer with θ = −150°. The higher stability of the dimer structure with θ = −94° is likely determined by symmetry and molecular packing induced by the opposite rotation of the corresponding dihedrals ($t-g+/t+g-$ side-chain orientation) (Figure 4).

As for dimer configurations, trimer conformers gg ($\theta = \theta'$ = 90°), tg (θ = 90°, θ' = 180°), and tt ($\theta = \theta'$ = 180°) were not displayed in the MMH output file. Vibrational frequency calculations for the optimized structures at M05-2X/6-31G-(d,p) give small imaginary frequency (1.9i cm^{-1}) for gg structure, whereas the tt conformer showed a second-order saddle point. Thus, only the gg trimer configuration is considered in this study.[81]

Inter-ring torsion angles (θ, θ') and the corresponding ΔE values of most stable trimer $\alpha-\alpha'Py_3SiOH$ structures (M05-2X/6-31G(d,p)//AM1), as well as of the gg conformer, are reported in Table 5 (Scheme 1). The corresponding optimized geometries are illustrated in Figure 6. Trimer conformers with ΔE < 5 kcal/mol correspond to $g-/cg+$, $g/tg+$, and to $tg-/tg+$ with θ = −107° and θ' = 99° being the latter the minimum structure as confirmed also by single-point energy calculations using 6-31++G(d,p) basis set. Closer examination of θ, θ' and ΔE (Table 5) indicates that the stability of trimer structures is not likely determined by inter-ring torsional angles. Note conformations $g+/tg+$ and gg with similar θ and θ' that differ in ΔE by more than 10 kcal/mol.

For the analysis of alkyl side chains orientation for a given trimer conformer, dihedral angles $\angle NC_\alpha C_\beta C_\gamma$ and $\angle C_\alpha C_\beta C_\gamma Si$ were determined in relation to θ for the first and second side chains (τ, τ' and ν, ν') and to θ' for the second and third side chains (τ', τ'' and ν', ν''), respectively. Figure 7 reports the dihedral angles for each conformation in the order of increasing ΔE (arrow on the top). τ and τ' markedly alternate between ≅ ±180° and $\tau' \cong \tau'' \leq -50°$ for less stable trimer structures, whereas no trend is evident for $\angle C_\alpha C_\beta C_\gamma Si$ (ν, ν' and ν', ν''). Combined analysis of $\angle NC_\alpha C_\beta C_\gamma$ and $\angle C_\alpha C_\beta C_\gamma Si$ for conformers with ΔE < 5 kcal/mol indicates paired rotations in opposite sense. As for dimer comformers, molecular packing

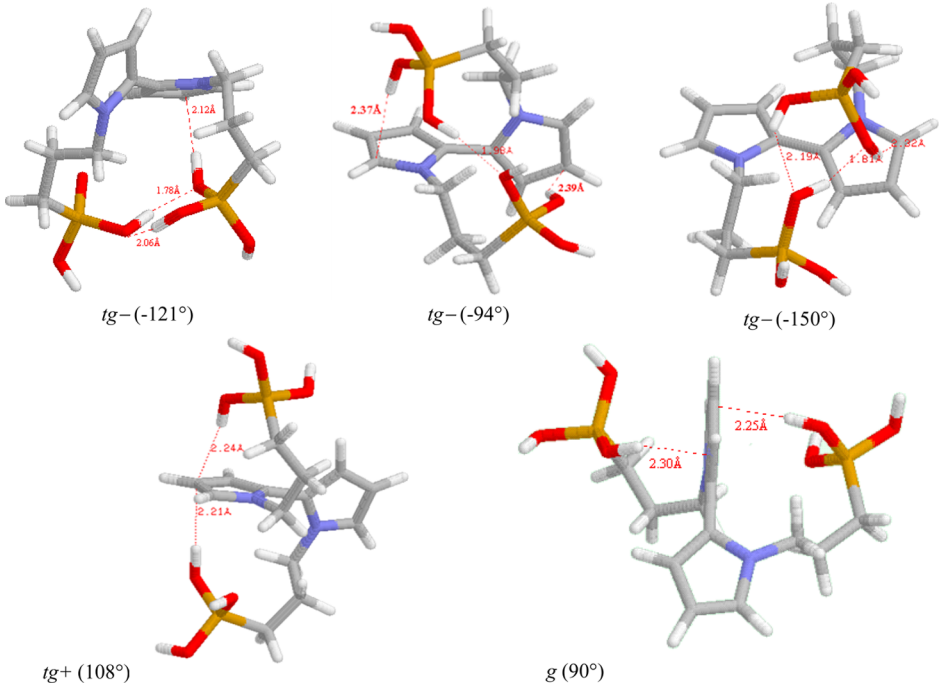

Figure 4. Optimized geometries at M05-2X/6-31G(d,p) of $\alpha-\alpha'Py_2SiOH$ dimer conformations that define the energy wells in Figure 3. Relevant donor−acceptor interactions with the corresponding interatomic distances are indicated.

DOI: 10.1021/acs.jpca.5b04167
J. Phys. Chem. A 2015, 119, 7038−7051

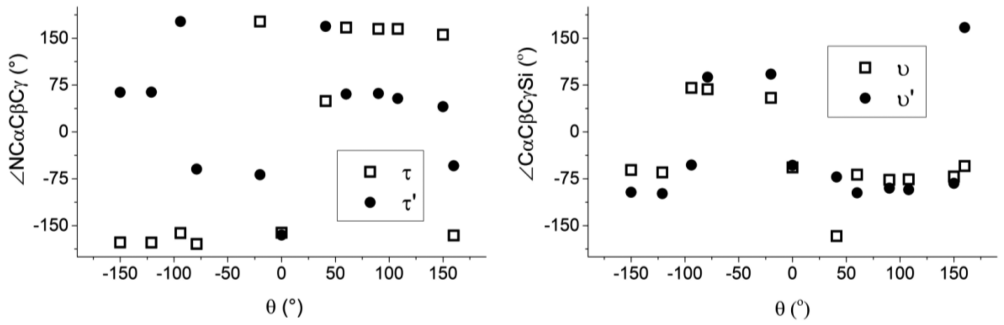

Figure 5. Dihedral angles $\angle NC_\alpha C_\beta C_\gamma$ (τ, τ') and $\angle C_\alpha C_\beta C_\gamma Si$ (ν, ν') of N-side chains of $\alpha-\alpha'Py_2SiOH$ structures as a function of the torsion angle at the M05-2X/6-31G(d,p) level of theory.

Table 5. Inter-Ring Torsional Angles (θ, θ') and Relative Energy (ΔE) of Trimer Py_3SiOH Conformations, As Obtained with M05-2X/6-31G(d,p)

conformation	θ (deg)	θ' (deg)	ΔE (kcal/mol)
g−/*cg*+	−93	70	0
g+/*tg*+	93	127	3.4
tg−/*tg*+	−107	99	3.6
	−135	116	7.6
	−115	110	10.9
gg	90	90	14.6

induced by alkyl side chains orientation provides stability to $\alpha-\alpha'Py_3SiOH$ (Figure 6).

Calculations of gap energy E_g and of global dipole moment of dimer and trimer structures at M05-2X/6-31G(d,p) level of theory indicate dipole-induced decrease of E_g for less stable structures (Figure 8). Conversely, either properties decrease or increase for a given minima structure (ΔE < 5 kcal/mol), regardless of ΔE and molecular packing. In addition, dimer (or trimer) structures with consistently different stability present similar dipole moments. No correlation was found between E_g and changes in ε_H, ε_L energy levels, even though the latter values indicated that the donor−acceptor character of PySiOH is preserved in $\alpha-\alpha'$ Py linked oligomers.

3.3. Noncovalent Interactions of $\alpha-\alpha'Py_nSiOH$. Table 6 summarizes the results of NBO analysis of $\alpha-\alpha'Py_2SiOH$ conformers with ΔE < 7 kcal/mol. The most relevant intermolecular interactions are indicated by the corresponding interatomic distances in Figure 4. Two types of stabilizing contributions are obtained: (i) $n(O)-\sigma^*_{OH}$ interactions between the oxygen lone pair and the σ antibonding orbital of the hydroxyl functionality of adjacent silanol groups, and (ii) $\pi_{ring}-\sigma^*_{OH}$ interactions that involve silanol group and the π-system of Py ring.[50,51,82] Minima *tg*− conformations (ΔE < 5 kcal/mol) present a higher charge transfer (Δq) and stabilization energy ($E^{(2)}$) for $n(O)-\sigma^*_{OH}$, in correlation with interatomic distances less than 2 Å. Conversely, dispersive $\pi_{ring}-\sigma^*_{OH}$ NBOs are more important for structures with ΔE > 5 kcal/mol (e.g., conformers *tg*+ and *g* in Table 6). Nonetheless, the contribution of these dispersive forces is non-negligible also for *tg*− structures, as indicated the evaluation of the relative importance of $n(O)-\sigma^*_{OH}$ and $\pi_{ring}-\sigma^*_{OH}$ following an elimination procedure implemented by NBO.[50,51] The energy contribution of the deleted term was estimated by the energy change (ΔE_{BD}) given by the difference between the energy of deletion (E_{elim}) and the original self-consistent field (SCF) energy (E_{totSCF}). For the *tg*− structure with θ = −121°, deletion of more important $n(O)-\sigma^*_{OH}$ and $\pi_{ring}-\sigma^*_{OH}$ interactions produces a destabilization of 20.5 and of 10.8 kcal/mol, respectively. Similarly, ΔE_{BD} of 2.1 and 10.1 kcal/mol were obtained for the *tg*− conformer with θ = −150°. Accordingly, elimination of either $n(O)-\sigma^*_{OH}$ or $\pi_{ring}-\sigma^*_{OH}$ NBOs causes a notable energetic impact on the *tg*− conformation stability, which points to a cooperative contribution of electrostatic and dispersive interactions. This is supported by the smaller contribution of $\pi_{ring}-\sigma^*_{OH}$ NBOs for the *tg*− structure with θ = −94° in comparison to the cases of the other two *tg*− conformers (Table 6). The former involves interactions between OH groups and Py rings of opposite PySiOH units (Figure 3). These cooperative weak interactions provide important stability to the *tg*− conformer (θ = −94°), being closer in ΔE to the minimum *tg*− conformer (θ = −121°) (Table 4).

Similar results are obtained for trimer configurations $\alpha-\alpha'Py_3SiOH$ (Table 7, Figure 6). Minima-energy conformers (ΔE < 5 kcal/mol) present smaller interatomic distances, higher $E^{(2)}$ and higher Δq for $n(O)-\sigma^*_{OH}$ interactions. Deletion of important $n(O)-\sigma^*_{OH}$ contributions produces an increase of ΔE_{BD} between 10 and 20 kcal/mol. Note that these interactions are not limited to silanol groups on adjacent side chains, as in the case of the minimum *g*−/*cg*+ structure (Figure 6).

The importance of weak noncovalent interactions is pointed out also by the increase of ΔE as the contribution of $\pi-\sigma^*_{OH}$ interactions decreases for a given minima conformer, as well as by the non-negligible $n(O)-\sigma^*_{OH}$ but less important $\pi_{ring}-\sigma^*_{OH}$ interaction for the *gg* conformer (ΔE > 10 kcal/mol). (Table 5).

The analysis of high-frequency vibrations involving the most important stabilizing $n(O)-\sigma^*_{OH}$ NBOs of dimer and trimer structures with ΔE < 5 kcal/mol indicated some correlation between $E^{(2)}$ and the stretching vibration of OH groups ν(OH). As shown in Figure 9, for *tg*− dimer structures with θ = −121° and θ = −150°, higher $E^{(2)}$ corresponds to higher intensity and smaller frequency of ν(OH), conversely to the *tg*− conformer with θ = −94° (Table 6). Dimer conformers *tg*+ and *g* with no important contribution of $n(O)-\sigma^*_{OH}$ showed even less intense vibrations at about 3700 cm^{-1} (free OH groups). Similarly, among the trimer structures, smaller frequency (3330 cm^{-1}) and higher intensity (≈800 km mol^{-1}) of ν(OH) is obtained for the *g*/*tg*+ conformer with stronger $n(O)-\sigma^*OH$ NBOs (Table 7), whereas the opposite was obtained for the minimum structure *g*−/*cg*+. This result points to oligomers stability being not solely determined by intramolecular H-boding interactions between silanol groups.

DOI: 10.1021/acs.jpca.5b04167
J. Phys. Chem. A 2015, 119, 7038−7051

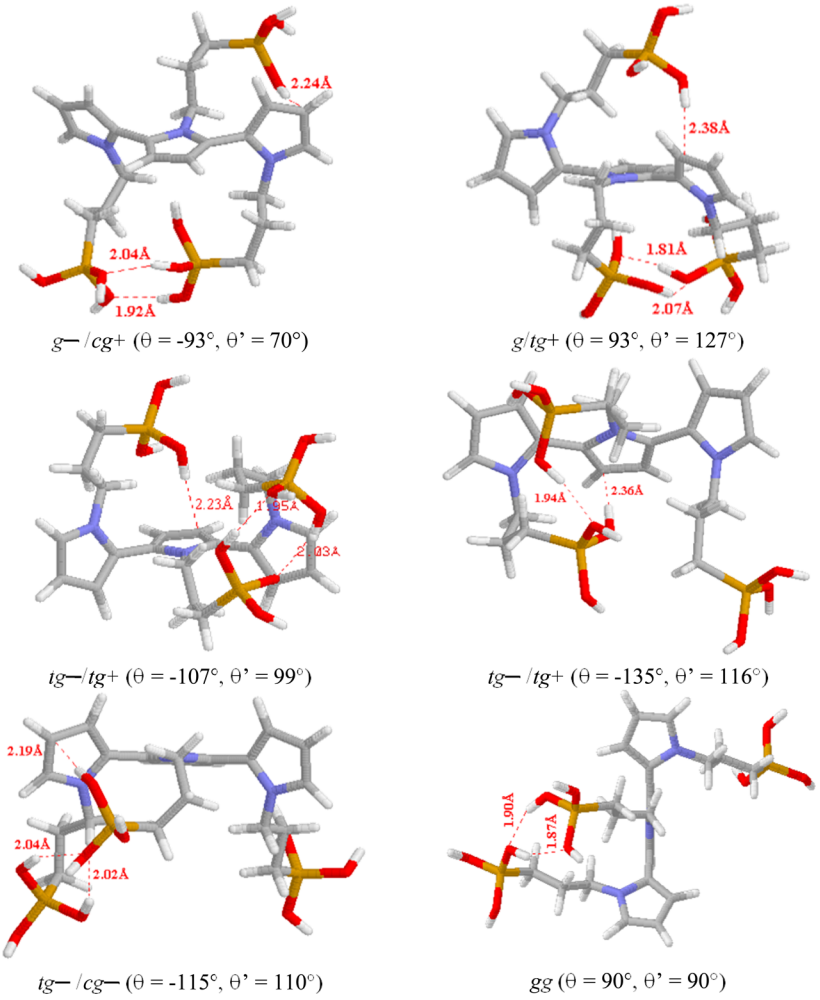

Figure 6. Optimized geometries of most stable trimer $\alpha-\alpha'Py_3SiOH$ conformations at the M05-2X/6-31G(d,p) level of theory. Relevant donor−acceptor interactions and the corresponding interatomic distances are indicated.

To understand better the nature of the above-mentioned stabilizing interactions, RDG analysis was carried out for most stable Py_nSiOH structures (ΔE < 5 kcal/mol). Figures 10 and 11 show RDG isosurfaces of dimer and trimer conformers. The blue color (ρ > 0, λ < 0) corresponds to strong attractive interactions (hydrogen bonding), green color ($\rho \cong 0$, $\lambda \cong 0$) to weak interactions (van der Waals), and red color (ρ > 0, λ > 0) to strong repulsive interactions. As expected, the latter are remarkable around bulky silicon atoms (steric crowding), whereas vdW forces expand among all C and H atoms belonging to the Py ring and alkyl side chains (green/light brown zones). In agreement with NBO results, strong intramolecular hydrogen bonding interactions between silanol groups (blue regions) are not limited to adjacent side chains in the case of trimer structures (Figure 11).

More importantly, intense blue-green regions between the interacting silanol group and Py ring (Figure 10) indicate dispersive interactions due to vdW forces resulting from induced deformation of the Py ring electronic cloud by the polar OH group of the electron-deficient SiOH. Note that the latter group is in antiparallel orientation with respect to the plane of the Py ring, thus obtaining T-shaped OH−π arrangements. By considering the dimer $tg-$ with $\theta = -94°$ and the minimum trimer structure $g-/cg+$ ($\theta = -93°$, $\theta' = 70°$), these present less strong electrostatic interactions but more balanced nonlocal vdW forces due to the higher molecular packing. Accordingly, the relative stability of minima structures is significantly enhanced by weak noncovalent vdW intramolecular interactions. Small Py_nSiOH oligomers can be visualized as noncovalent aromatic complexes driven by hydrogen-bonding and dispersive vdW-type forces.[83,84] Structures with important interactions involving T-shaped OH−π arrangements seems to be energetically favored due to the minimized repulsion but good dispersion and electrostatic interactions (2.1−2.4 Å).

Recall in Figure 8, structures with higher molecular packing, i.e., $tg-$ with $\theta = -94°$ and $g-/cg+$ ($\theta = -93°$, $\theta' = 70°$), present higher dipole moments and E_g values, in comparison to the data for other minima structures (ΔE < 5 kcal/mol). On the basis of NBO and RDG results (Figures 10 and 11), the increase of global dipole moment correlates with the higher contribution of "free" OH groups, whereas that of E_g with the less favored T-shaped OH−π arrangement. Accordingly, the decrease of the gap energy seems to be dominated by dispersive $\pi_{ring}-\sigma^*_{OH}$ interactions in favor of electron delocalization as a result of the donor−acceptor character of PySiOH units. The importance of dispersive vdW interactions on band gap modifications has been addressed for other oligomeric and macromolecular systems.[85]

DOI: 10.1021/acs.jpca.5b04167
J. Phys. Chem. A 2015, 119, 7038−7051

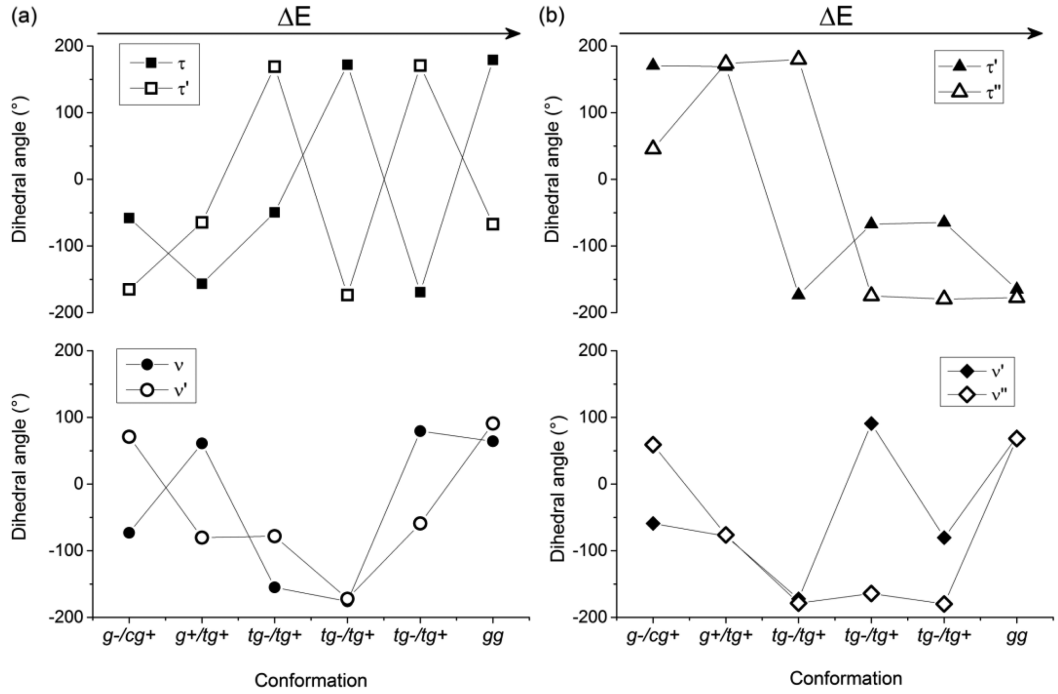

Figure 7. N-side chain dihedral angles of trimer $\alpha-\alpha'Py_3SiOH$ structures (M05-2X/6-31G(d,p)//AM1): (a) $\angle NC_\alpha C_\beta C_\gamma$ (τ, τ') and $\angle C_\alpha C_\beta C_\gamma Si$ (ν, ν') in relation to θ between the first and second Py rings; (b) $\angle NC_\alpha C_\beta C_\gamma$ (τ', τ'') and $\angle C_\alpha C_\beta C_\gamma Si$ (ν', ν'') in relation to θ' between the second and third Py rings. Arrows on the top indicate increasing relative energy (Table 5).

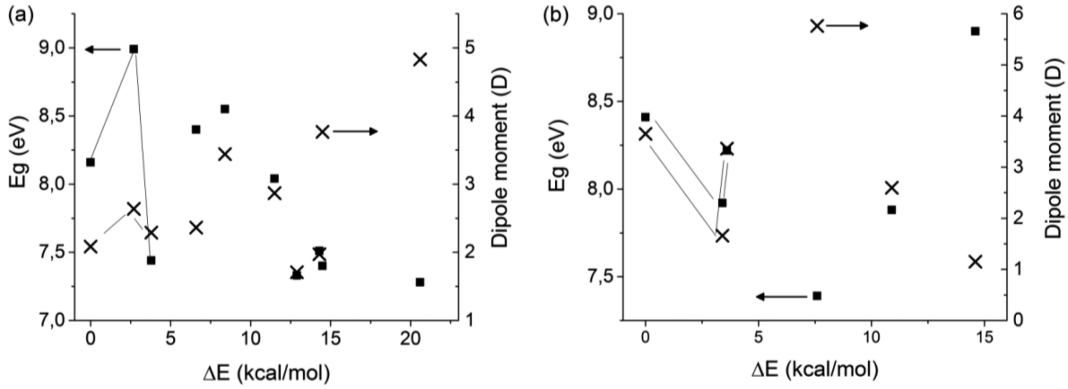

Figure 8. Band gap energy E_g (closed squares) and dipole moment (crosses) at M05-2X/6-31G(d,p) as a function of ΔE for (a) dimer and (b) trimer structures (Tables 4 and 5).

Table 6. Natural Bond Orbital (NBO) Analysis at the M05-2X/6-31G(d,p) Level of Theory for Dimer Py_2SiOH Conformations Defining Potential Energy Wells in Figure 3

conformation (ΔE in kcal/mol)	θ (deg)	donor NBOs	acceptor NBOs	distance (Å)	$E^{(2)}$ (kcal/mol)	Δq (au)
tg− (0)	−121	n(O)	O−H σ^*	1.78	20.7	0.033
				2.06	3.8	0.006
		π	O−H σ^*	2 0.12	10.3	0.019
(2.7)	−94	n(O)	O−H σ^*	1.98	10.4	0.013
		π	O−H σ^*	2.37	3.9	0.007
				2.39	2.5	0.005
(3.8)	−150	n(O)	O−H σ^*	1.81	18.1	0.029
				2.19	2.0	0.003
		π	O−H σ^*	2.33	9.8	0.018
g (5.8)	90	π	O−H σ^*	2.25	5.9	0.01
				2.30	4.9	0.009
tg+ (6.6)	108	π	O−H σ^*	2.21	5.4	0.01
				2.24	3.8	0.007

DOI: 10.1021/acs.jpca.5b04167
J. Phys. Chem. A 2015, 119, 7038−7051

Table 7. Natural Bond Orbital (NBO) Analysis at the M05-2X/6-31G(d,p) Level of Theory for Trimer Py_3SiOH Conformers

conformer (ΔE in kcal/mol)	θ, θ' (deg)	donor NBOs	acceptor NBOs	distance (Å)	$E^{(2)}$ (kcal/mol)	Δq (au)
g−/*cg*+	−93, +70	n(O)	O−H σ^*	1.92	13.1	0.017
(0)				2.04	4.5	0.007
		π	O−H σ^*	2.24	5.5	0.010
				2.31	2.6	0.005
g+/*tg*+	93, 127	n(O)	O−H σ^*	1.81	18.1	0.029
(3.4)				2.07	3.4	0.006
		π	O−H σ^*	2.20	9.8	0.018
				2.38	2.8	0.005
tg−/*tg*+	−107, +99	n(O)	O−H σ^*	1.95	8.4	0.013
(3.6)				2.03	3.5	0.006
		π	O−H σ^*	2.23	3.5	0.006
				2.30	3.5	0.006
tg−/*tg*+	−135, +116	n(O)	O−H σ^*	1.94	12.2	0.016
(7.6)		π	O−H σ^*	2.36	4.2	0.008
tg−/*tg*+	−115, +110	n(O)	O−H σ^*	2.02	2.4	0.004
(10.9)				2.03	3.3	0.005
		π	O−H σ^*	2.19	6.7	0.012
gg	90, 90	n(O)	O−H σ^*	1.87	6.9	0.011
(14.6)				1.90	11.3	0.018

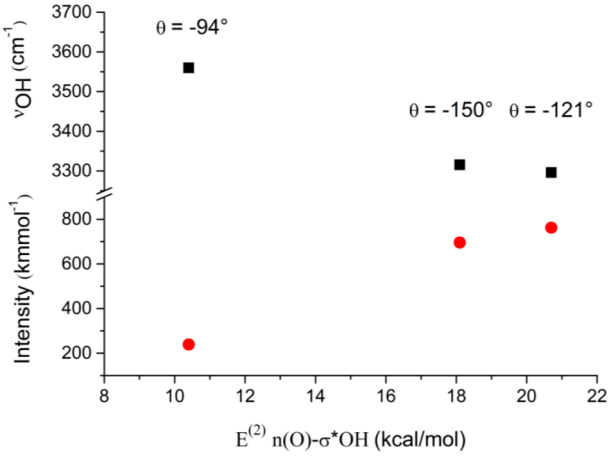

Figure 9. Relationships of theoretical ν_{OH} frequency (■) and intensity (●) with perturbative energy $E^{(2)}$ (kcal/mol) of n(O)−σ^*_{OH} intramolecular interactions at the M05-2X/6-31G/d,p) level of theory for *tg*− α−α' Py_2SiOH conformers.

3.4. Summarized Experimental Chemical Behavior of PySi Solution. As mentioned before, quite peculiar chemical behavior of PySi in methanol-based solutions (4 vol % of PySi methanol/water 95:5, pH ≅ 4 by adding few drops of acetic acid) has been revealed by different spectroscopic analyses (ATR-IR, NMR (^{1}H,^{13}C,^{29}Si), UV−vis).[1,3,7] ATR-IR experiments indicated formation of hydrogen bonded-silicon and siloxane linkages, according to the broad bands between 3600−3100 cm^{-1}/900−800 cm^{-1} (OH stretching/deformation) and 1100−1050 cm^{-1} (Si−O−Si stretching). However, differently from methyltrimethoxysilane, which was studied in parallel using similar experimental conditions, condensation of silanol groups is less favored for PySi solution, as manifested by the negligible variation of ν(OH) with time.[1] Note that hydrogen bonding interactions between SiOH and polar solvent molecules cannot be neglected for both silanes. Concerning Py ring vibrations, α−α' linking of Py units was indicated by.the more important increase of the band at 800 cm^{-1} in relation to the shoulder at 695 cm^{-1}, associated with Py "bulk" (B) and "end groups" (T) modes, respectively.

Similar considerations were derived from NMR experiments (using deuterated solvents and acid). In particular, ^{29}Si NMR spectra after 1 month of PySi solution preparation[3] showed an intense peak at −48.9 ppm associated with siloxane dimer R−Si(−O−Si)$(OH)_2$ (T_1 structure) and less important peaks at −40.5 and −58.0 ppm corresponding to hydrolyzed silane R−Si$(OH)_3$ (T_H) and linear siloxane chain R−Si(−O−Si)$_2$(OH) (T_2).[86] Conversely, T2 structures and tridimensional cross-linking prevail for a similarly prepared solution of dihydroimidazole based silane, namely *N*-[3-(triethoxysilyl)propyl]-dihydroimidazole. Note that dihydroimidazole is a nonaromatic five-membered heterocyle with two nitrogen atoms. ^{1}H NMR spectra (Figure 12) show a remarkable increase with the time of the peak at 4.86 ppm, related to the formation of SiOD.[86] Due to the use of deuterated solvents, this peak does not shift toward smaller δ with time, as expected for hydrogen-bonded silicon. More importantly, the decrease and broadening of the H−C_α peak at 6.67 ppm with time is remarkable in comparison to that of H−C_β (6.02 ppm) (Figure 12). Closer examination of the H−C_α peak evolution revealed two additional shoulders at 6.65 and 6.63 ppm for a 2-month aged solution, indicating formation of oligomeric α−α' linked Py structures.[87] This was indicated also by the more important variation with time of the C_α peak (119.4 ppm) in relation to the C_β peak (106.03 ppm) in the ^{13}C NMR spectra.[88]

With regard to the UV−vis spectra, these were recorded also for pyrrole, using similarly prepared solutions.[3] As shown in Figure 13, both Py and PySi solutions show two overlapped features between 400 and 550 nm, in addition to a band at about 600 nm, for relatively short times of solutions preparation. In the case of the PySi solution, these features are detected at higher wavelength due to N-substitution but are much more intense (for equivalent times), suggesting intramolecular polarization and/or medium-induced polarization effects. This points to hydrolyzed PySi linking via Py rings to form charged species composed of Py_nSiOH oligomers. At longer times, the overlapped peaks (400−550 nm) evolve toward an intense broad sub-bands feature, which progressively

DOI: 10.1021/acs.jpca.5b04167
J. Phys. Chem. A 2015, 119, 7038−7051

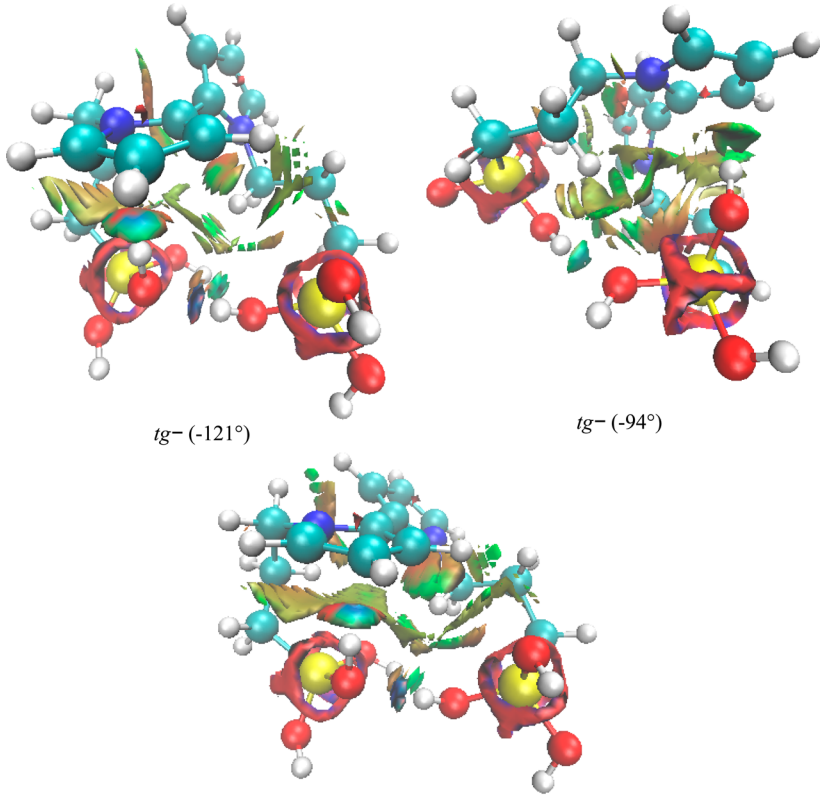

Figure 10. Gradient isosurfaces (s = 0.5 au) for the minima energy dimer conformers Py_2SiOH at the M05-2X/6-31G(d,p). The surfaces on a blue-green-red scale from $-0.05 < \text{sign}(\lambda_2)\ \rho(r) < +0.05$ au.

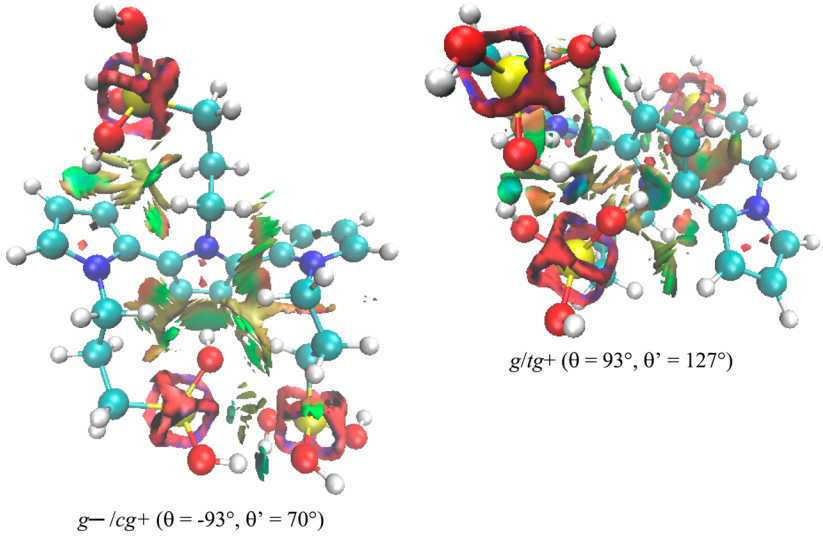

Figure 11. Gradient isosurfaces (s = 0.5 au) for the minima energy trimer conformers Py_3SiOH at the M05-2X/6-31G(d,p). The surfaces on a blue-green-red scale from $-0.05 < \text{sign}(\lambda_2)\ \rho(r) < +0.05$ au.

shifts to smaller wavelengths and tends to merge with the growing absorption tail.

Considering the above-presented theoretical results, the spectral evolution of PySi solution is dominated by the $\sigma-\pi$ mixing effect associated with OH$-\pi$ interactions. These not only limit silanol-end-group condensation but favor charge trapping due to charge-pinning action of electron-deficient SiOH promoting Py ring saturation. This consideration could explain the n-type semiconducting behavior of the PySi hybrid film.[7] In an effort to understand better the charge trapping phenomena, excited monomers and oligomers are currently investigated by time dependent DFT.

4. CONCLUSIONS

Pyrrolyl−silicon compounds, namely, PySi and PySiOH monomers, as well as $\alpha-\alpha'Py_nSiOH$ oligomers, were modeled and investigated using different theoretical approaches. PySiOH has a smaller gap energy and is more reactive than PySi due to

DOI: 10.1021/acs.jpca.5b04167
J. Phys. Chem. A 2015, 119, 7038−7051

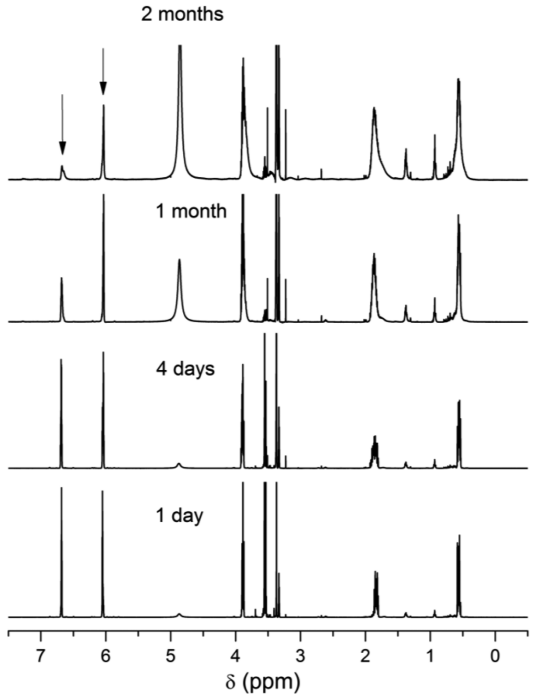

Figure 12. ^{1}H NMR spectra as a function of time of PySi solution, which was composed of 4 vol % of *N*-3-(trimethoxysilyl)pyrrole (>98%, Fluorochem) in high-purity (99.9%, Sigma-Aldrich) methanol-d_4 and deutrated water (95:5). A given amount of acetic acid-d_4 (99.9%, Sigma-Aldrich) was added for pH adjustment to ≅4. Spectra were recorded at room temperature using a Bruker 500 spectrometer (500.13 MHz) and standard 5 mm BB (broad-band) probe.

its donor−acceptor character with two preferential reactive sites: electron-rich Py ring and electron-deficient silanol end group. The decrease of the gap energy is determined by the decrease of the LUMO energy level, thus predicting favored delocalization of the conduction band. Conformational, NBO, and RDG analyses of $\alpha-\alpha'Py_nSiOH$ oligomers indicate enhanced stability by molecular packing and by cooperative intramolecular noncovalent interactions. Weak dispersive vdW interactions have their origin on the donor−acceptor character of PySiOH, where electron-deficient silanol induces deformation of Py electronic cloud. The electron delocalization favored this way determines the decrease of the gap energy of $\alpha-\alpha'Py_nSiOH$ oligomers. The present theoretical findings support the experimental behavior of PySi solution.

■ ASSOCIATED CONTENT

Supporting Information

Tables of bond lengths, bond and dihedral angles, and theoretical frequencies, intensities, and mode descriptions. Figure of frontier orbital maps. The Supporting Information is available free of charge on the ACS Publications website at DOI: 10.1021/acs.jpca.5b04167.

■ AUTHOR INFORMATION

Corresponding Author

*M. Trueba. E-mail: monica.trueba@unimi.it.

Author Contributions

The manuscript was written through contributions of all authors. All authors have given approval to the final version of the manuscript.

Notes

The authors declare no competing financial interest.

■ REFERENCES

(1) Trueba, M.; Trasatti, S. P. Pyrrole-Based Silane Primer for Corrosion Protection of Commercial Al alloys. Part I: Synthesis and Spectroscopic Characterization. *Prog. Org. Coat.* **2009**, *66*, 254−264.

(2) Trueba, M.; Trasatti, S. P. Pyrrole-Based Silane Primer for Corrosion Protection of Commercial Al alloys. Part II. Corrosion Performance in Neutral NaCl Solution. *Prog. Org. Coat.* **2009**, *66*, 265−275.

(3) Trueba, M.; Trasatti, S. P.; Flamini, D. O. Hybrid Coatings Based on Conducting Polymers and Polysiloxane Chains for Corrosion Protection of Al alloys. *Adv. Mater. Res.* **2010**, *138*, 63−78.

(4) Flamini, D. O.; Trueba, M.; Trasatti, S. P. Aniline-Based Silane as a Primer for Corrosion Inhibition of Aluminium. *Prog. Org. Coat.* **2012**, *74*, 302−310.

(5) Trueba, M.; Trasatti, S. P.; Flamini, D. O. The Effect of Aluminium Alloy Secondary Phases on Aniline-Based Silane Protection Capacity. *Corros. Sci.* **2012**, *63*, 59−70.

(6) Bianchi, S.; Trueba, M.; Trasatti, S. P.; Madaschi, E.; Sala, M. C. An In-Depth Comprehension of the Protection Mechanism of Al Alloys by Aniline-Based Silane. *Prog. Org. Coat.* **2014**, *77*, 2064−2075.

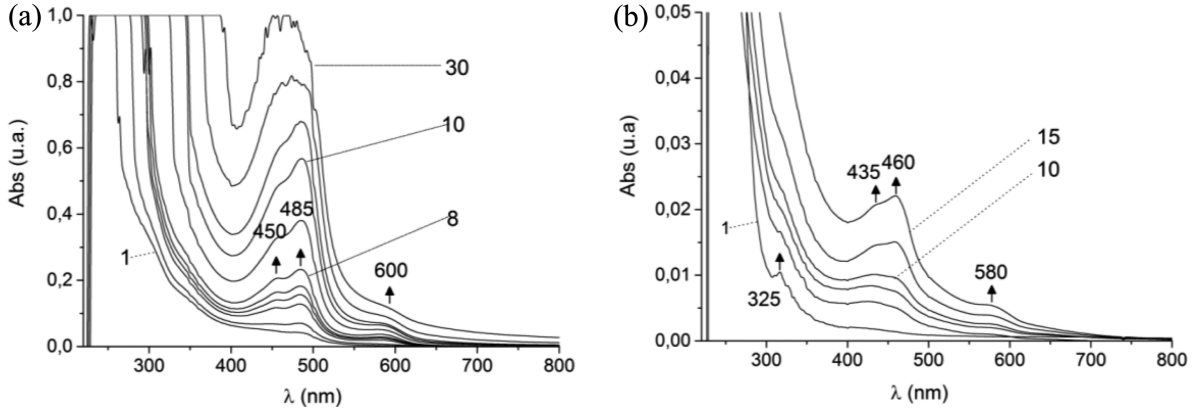

Figure 13. UV−vis spectra as a function of time of (a) PySi solution, which was prepared as for NMR experiments but using methanol (99.8%, Sigma-Aldrich), acetic acid (99.7%, Sigma-Aldrich), and water of quality Milli-Q. A similarly prepared solution of Py (b), using freshly distilled pyrrole monomer, was studied in parallel. Numbers in (a, b) indicate time in days. Spectra were recorded using a JASCO V530 spectrometer in the wavelength scan mode (200−800 nm).

DOI: 10.1021/acs.jpca.5b04167
J. Phys. Chem. A 2015, 119, 7038−7051

(7) Bertoli, I.; Trueba, M.; Trasatti, S. P. Electrical and Semiconducting Properties of Hydrid Films Deposited on Al 2024 (to be submitted for publication).
(8) Sulpizi, M.; Gaigeot, M.-P.; Sprik, M. The Silica−Water Interface: How the Silanols Determine the Surface Acidity and Modulate the Water Properties. *J. Chem. Theory Comput.* **2012**, *8*, 1037−1047.
(9) Sheldon, R.; Arends, I. W. C. E.; Hanefeld, U. *Green Chemistry and Catalysis*; Wiley-VCH Verlag GmbH: Weinheim: Germany, 2007.
(10) Vach, H. Electron-Deficiency Aromaticity in Silicon Nanoclusters. *J. Chem. Theory Comput.* **2012**, *8*, 2088−2094.
(11) Heinze, J.; Frontana-Uribe, B. A.; Ludwigs, S. Electrochemistry of Conducting Polymers—Persistent Models and New Concepts. *Chem. Rev.* **2010**, *110*, 4724−4771.
(12) Boiadjiev, S. E.; Lightner, D. A. Optical Activity and Stereochemistry of Linear Oligopyrroles and Bile Pigments. *Tetrahedron: Asymmetry* **1999**, *10*, 607−655.
(13) Liu, X.-T.; Guo, J.-F.; Ren, A.-M.; Xu, Z.; Huang, S.; Feng, J.-K. Theoretical Insight into Linear Optical and Two-Photon Absorption Properties for a Series of N-arylpyrrole-Based Dyes. *Org. Biomol. Chem.* **2012**, *10*, 7527−7535.
(14) Salzner, U.; Lagowski, J. B.; Pickup, P. G.; Poirier, R. A. Theoretical Analysis of Effects of p-Conjugating Substituents on Building Blocks for Conducting Polymers. *J. Org. Chem.* **1999**, *64*, 7419−7425.
(15) Salzner, U.; Kızıltepe, T. Theoretical Analysis of Substituent Effects on Building Blocks of Conducting Polymers. 3,4′-Substituted Bithiophenes. *J. Org. Chem.* **1999**, *64*, 764−769.
(16) Hutchison, G. R.; Ratner, M. A.; Marks, T. J. Accurate Prediction of Band Gaps in Neutral Heterocyclic Conjugated Polymers. *J. Phys. Chem. A* **2002**, *106*, 10596−10605.
(17) Hutchison, G. R.; Ratner, M. A.; Marks, T. J. Intermolecular Charge Transfer Between Heterocyclic Oligomers. Effects of Heteroatom and Molecular Packing on Hopping Transport in Organic Semiconductors. *J. Am. Chem. Soc.* **2005**, *127*, 16866−16881.
(18) Costanzo, F.; Tonelli, D.; Scalmani, G.; Cornil, J. Theoretical Investigation of the Electronic and Optical Properties of Oligothiophenes upon Methyl, Thiol, and Thiomethyl Substitutions. *Polymer* **2006**, *47*, 6692−6697.
(19) Ashby, B. A. Preparation, Chemistry and Spectra of (Silylmethyl)-Pyrroles. *J. Organomet. Chem.* **1966**, *5*, 405−412.
(20) Rabias, I.; Hamerton, I.; Howlin, B. J. Theoretical Studies of Conducting Polymers Based on Substituted Polypyrroles. *Comput. Theor. Polym. Sci.* **1998**, *8*, 265−271.
(21) Voronkov, M. G.; Trofimova, O. M.; Turchaninov, V. K.; Zel'bst, E. A.; Bolgova, Y. I.; Belyaeva, V. V.; Larina, L. I.; Aksamentova, T. N.; Mikhaleva, A. I.; Chernov, N. F. N-silatranylmethyl Derivatives of Pyrrole, Indole, and Carbazole. *Russ. J. Org. Chem.* **2003**, *39*, 1458−1466.
(22) Casanovas, J.; Cho, L. Y.; Ocampo, C.; Aleman, C. A Theoretical Study of the Effects Produced by N-hydroxyalkyl Substitution in Pyrrole Oligomers. *Synth. Met.* **2005**, *151*, 239−245.
(23) Geerlings, P.; De Proft, F.; Langenaeker, W. Conceptual Density Functional Theory. *Chem. Rev.* **2003**, *103*, 1793−1874.
(24) Clark, G. R.; Ferguson, L. A.; McIntosh, A. E.; Sohnel, T.; Wright, L. J. Functionalization of Metallabenzenes through Nucleophilic Aromatic Substitution of Hydrogen. *J. Am. Chem. Soc.* **2010**, *132*, 13443−13452.
(25) Fuentealba, P.; Florez, E.; Tiznado, W. Topological Analysis of the Fukui Function. *J. Chem. Theory Comput.* **2010**, *6*, 1470−1478.
(26) Beker, W.; Szarek, P.; Komorowski, L.; Lipinski, J. Reactivity Patterns of Imidazole, Oxazole, and Thiazole as Reflected by the Polarization Justified Fukui Functions. *J. Phys. Chem. A* **2013**, *117*, 1596−1600.
(27) Sánchez-Bojorge, N. A.; Flores-Holguín, N.; Glossman-Mitnik, D.; Rodríguez-Valdez, L. M. Computational Note on the Chemical Reactivity of Pyrrole Derivatives. *J. Mol. Struct.: THEOCHEM* **2009**, *912*, 119−120.
(28) Osorio, E.; Ferraro, M. B.; Oña, O. B.; Cardenas, C.; Fuentealba, P.; Tiznado, W. Assembling Small Silicon Clusters Using Criteria of Maximum Matching of the Fukui Functions. *J. Chem. Theory Comput.* **2011**, *7*, 3995−4001.
(29) Galvan, M.; Dal pino, A., Jr.; Joannopoulos, J. D. Hardness and Softness in the ab initio Study of Polyatomic Systems. *Phys. Rev. Lett.* **1993**, *70*, 21−24.
(30) Montero, L. A.; Esteva, A. M.; Molina, J.; Zapardiel, A.; Hernandez, L.; Marquez, H.; Acosta, A. A Theoretical Approach to Analytical Properties of 2,4-Diamino-5-Phenylthiazole in Water Solution. Tautomerism and Dependence on pH. *J. Am. Chem. Soc.* **1998**, *120*, 12023−12033.
(31) Montero, L. A.; Molina, J.; Fabian, J. Multiple Minima Hypersurfaces of Water Clusters for Calculations of Association Energy. *Int. J. Quantum Chem.* **2000**, *79*, 8−16.
(32) Codorniu-Hernandez, E.; Mesa-Ibirico, A.; Hernandez-Santiesteban, R.; Montero-Cabrera, L. A.; Martinez-Luzardo, F.; Santana-Romero, J. L.; Borrmann, T.; Stohrer, W. D. Essential Amino Acids Interacting with Flavonoids: A Theoretical Approach. *Int. J. Quantum Chem.* **2005**, *103*, 82−104.
(33) Crespo-Otero, R.; Perez-Badell, Y.; Padron-Garcia, J. A.; Montero-Cabrera, L. A. Exploring the Potential Energy Surfaces of Association of NO with Aminoacids and Related Organic Functional Groups: The role of Entropy of Association. *Theor. Chem. Acc.* **2007**, *118*, 649−663.
(34) Morera-Boado, C.; Alonso-Becerra, E.; Montero-Cabrera, L. A.; González-Jonte, R. Validation of Performances of Some Semiempirical Hamiltonians for Predicting Molecular Structure Calculation of Natural Brassinosteroids: Towards Understanding their Biological Activity by Electron Exchange Effect. *J. Mol. Struct.: THEOCHEM* **2007**, *819*, 109−120.
(35) Montero-Cabrera, L. A.; Perez-Badell, Y.; Mora-Fonz, M. J. An Approach to Hydration of Model Silica Materials by Exploring their Multiple Minima Hypersurfaces. The Role of Entropy of Association. *J. Phys. Chem. A* **2008**, *112*, 2880−2887.
(36) Perez-Labrada, K.; Brouard, I.; Morera, C.; Estevez, F.; Bermejo, J.; Rivera, D. G. Click' Synthesis of Triazole-Based Spirostan Saponin Analogs. *Tetrahedron* **2011**, *67*, 7713−7727.
(37) Pérez-Labrada, K.; Morera-Boado, C.; Brouard, I.; Llerena, R.; Rivera, D. G. Synthesis and Conformational Study of Triazole-linked Bis-Spirostanic Conjugates. *Tetrahedron Lett.* **2013**, *54*, 1602−1606.
(38) Ruíz, A.; Morera-Boado, C.; Almagro, L.; Coro, J.; Maroto, E. E.; Herranz, M.; Filippone, S.; Molero, D.; Martínez-Álvarez, R.; Garcia, de la Vega; et al. Dumbbell-Type Fullerene-Steroid Hybrids: A Join Experimental and Theoretical Investigation for Conformational, Configurational, and Circular Dichroism Assignments. *J. Org. Chem.* **2014**, *79*, 3473−3486.
(39) Dewar, M. J. S.; Thiel, W. Ground-States of Molecules. 38. Mndo Method - Approximations and Parameters. *J. Am. Chem. Soc.* **1977**, *99*, 4899−4907.
(40) Stewart, J. J. P. Optimization of Parameters for Semiempirical Methods I. Method. *J. Comput. Chem.* **1989**, *10*, 209−220.
(41) Stewart, J. J. P. *MOPAC2009*, Version 10.250W; Stewart Computational Chemistry, 2009 (http://OpenMOPAC.net).
(42) Becke, A. D. J. Density-Functional Thermochemistry. 4. A New Dynamical Correlation Functional and Implications for Exact-Exchange Mixing. *J. Chem. Phys.* **1996**, *104*, 1040−1046.
(43) Zhao, Y.; Schultz, N. E.; Truhlar, D. G. Design of Density Functionals by Combining the Method of Constraint Satisfaction with Parametrization for Thermochemistry, Thermochemical Kinetics, and Noncovalent Interactions. *J. Chem. Theory Comput.* **2006**, *2*, 364−382.
(44) Zhao, Y.; Truhlar, D. G. Exploring the Limit of Accuracy of the Global Hybrid Meta Density Functional for Main-Group Thermochemistry, Kinetics, and Noncovalent Interactions. *J. Chem. Theory Comput.* **2008**, *4*, 1849−1868.
(45) Frisch, M. J.; Trucks, G. W.; Schlegel, H. B.; Scuseria, G. E.; Robb, M. A.; Cheeseman, J. R.; Scalmani, G.; Barone, V.; Mennucci, B.; Petersson, G. A.; et al. *Gaussian 09*, Revision D.01; Gaussian, Inc.: Wallingford, CT, 2009.
(46) Marenich, A. V.; Cramer, C. J.; Truhlar, D. G. *CM5PAC*; University of Minnesota: Minneapolis, 2011.

DOI: 10.1021/acs.jpca.5b04167
J. Phys. Chem. A 2015, 119, 7038−7051

(47) Marenich, A. V.; Jerome, S. V.; Cramer, C. J.; Truhlar, D. G. Charge model 5: An Extension of Hirshfeld Population Analysis for the Accurate Description of Molecular Interactions in Gaseous and Condensed Phases. *J. Chem. Theory Comput.* **2012**, *8*, 527−541.
(48) Hirshfeld, F. L. Bonded-Atom Fragments for Describing Molecular Charge Densities. *Theoret. Chim. Acta* **1977**, *44*, 129−138.
(49) http://karin.fq.uh.cu/mmh/ 2009 (available by request).
(50) Glendening, E. D.; Reed, A. E.; Carpenter, J. E.; Weinhold, F. *NBO* Version 3.1.
(51) Glendening, E. D.; Reed, A. E.; Carpenter, J. E.; Weinhold, F. *NBO 3.0 Program Manual*; Gaussian books: Wallingford, CT, 1989.
(52) Johnson, R.; Keinan, S.; Mori-Sánchez, P.; Contreras-García, J.; Cohen, A. J.; Yang, W. Revealing Noncovalent Interactions. *J. Am. Chem. Soc.* **2010**, *132*, 6498−6506.
(53) Vedha, S. A.; Solomon, R. V.; Venuvanalingam, P. On the Nature of Hypercoordination in Dihalogenated Perhalocyclohexasilanes. *J. Phys. Chem. A* **2013**, *117*, 3529−3538.
(54) Cohen, A. J.; Mori-Sánchez, P.; Yang, W. Insights Into Current Limitations of Density Functional Theory. *Science* **2008**, *321*, 792−794.
(55) *Handbook of Chemistry and Physics*, 84th ed.; CRC Press, LLC: Boca Raton, FL, 2004.
(56) Takeuchi, H.; Inoue, K.; Enmi, J.; Hamada, T.; Shibuya, T.; Konaka, S. Molecular Structure of N-methylpyrrole Studied by Gas Electron Diffraction Using Rotational Constants and Liquid−Crystal NMR Spectroscopy. *J. Mol. Struct.* **2001**, *567*−*568*, 107−111.
(57) Kofranek, M.; Kovar, T.; Karpfen, A.; Lischka, H. Ab Initio Studies on Heterocyclic Conjugated Polymers: Structure and Vibrational Spectra of Pyrrole, Oligopyrroles and Polypyrrole. *J. Chem. Phys.* **1992**, *96*, 4464−4473.
(58) Porezag, D.; Frauenheim, Th.; Kohler, Th.; Seifert, G.; Kaschner, R. Construction of Tight-Binding-Like Potentials on the Basis of Density-Functional Theory: Application to Carbon. *Phys. Rev. B: Condens. Matter Mater. Phys.* **1995**, *5*, 12947−12957.
(59) Nyburg, S. C.; Lüth, H. n-Octadecane: A Correction and Refinement of the Structure Given by Hayashida. *Acta Crystallogr., Sect. B: Struct. Crystallogr. Cryst. Chem.* **1972**, *B28*, 2992−2995.
(60) Hayashi, M.; Nakagawa, J.; Aguni, Y. Microwave Spectrum of Propyl Silane. *Bull. Chem. Soc. Jpn.* **1980**, *53*, 2468−2471.
(61) Blake, A. J.; Ebsworth, E. A. V.; Henderson, S. G. D.; Dyrbusch, M. Structure of Methoxysilane at 110 K. *Acta Crystallogr., Sect. C: Cryst. Struct. Commun.* **1988**, *C44*, 1−3.
(62) Krishnan, R.; Binkley, J. S.; Seeger, R.; Pople, J. A. Selfconsistent Molecular Orbital Methods. XX. A Basis Set for Correlated Wave Functions. *J. Chem. Phys.* **1980**, *72*, 650−654.
(63) Trofimov, A. B.; Schirme, J. Polarization Propagator Study of Electronic Excitation in Key Heterocyclic Molecules. I. Pyrrole. *Chem. Phys.* **1997**, *214*, 153−170.
(64) Chieh, Y. C.; Chen, P. C.; Chen, S. C. Theoretical Study of the Internal Rotational Barriers in some N-substituted Nitropyrroles. *J. Mol. Struct.: THEOCHEM* **2003**, *636*, 115−123.
(65) Anderson, D. G.; Rankin, D. W. H. Determination of the Gas-Phase Molecular Structures of Methyldisilylamine and Ethyldisilylamine by Electron Diffraction. *J. Mol. Struct.* **1989**, *195*, 261−270.
(66) Mellouki, A.; Auwera, J. V.; Herman, M. Rotation-Vibration Constants for the nu1, nu22, nu24, nu22 + nu24, and Ground States in Pyrrole (12C4H5N). *J. Mol. Spectrosc.* **1999**, *193*, 195−203.
(67) Mellouki, A.; Lievin, J.; Herman, M. The Vibrational Spectrum of Pyrrole (C4H5N) and Furan (C4H4O) in the gas phase. *Chem. Phys.* **2001**, *271*, 239−266.
(68) Palmer, M. H. The High Resolution Infrared Spectrum of Pyrrole Between 900 and 1500 cm^{-1} Revisited. *J. Mol. Spectrosc.* **2008**, *252*, 93−97.
(69) Lee, S. Y.; Boo, B. H. Molecular Structures and Vibrational Spectra of Pyrrole and Carbazole by Density Functional Theory and Conventional ab initio Calculations. *J. Phys. Chem.* **1996**, *100*, 15073−15078.
(70) Massoumi, B.; Isfahani, N. S.; Saraei, M.; Entezami, A. Investigation of the Electroactivity, Conductivity, and Morphology of Poly(pyrrole-co-N-alkyl pyrrole) Prepared via Electrochemical Nanopolymerization and Chemical Polymerization. *J. Appl. Polym. Sci.* **2012**, *124*, 3956−3962.
(71) Montejo, M.; Partal Urena, F.; Marquez, F.; Lopez Gonzalez, J. J. Triethylsilanol: Molecular Conformations and Role of the Hydrogen-Bonding Oligomerization in its Vibrational Spectra. *J. Phys. Chem. A* **2008**, *112*, 1545−1551.
(72) Zotti, G.; Martina, S.; Wegner, G.; Schluter, A. D. Well-Defined Pyrrole Oligomers: Electrochemical and UV/vis Studies. *Adv. Mater.* **1992**, *4*, 798−781.
(73) Salzner, U.; Pickup, P. G.; Poirier, R. A.; Lagowski, J. B. Accurate Method for Obtaining Band Gaps in Conducting Polymers Using a DFT/Hybrid Approach. *J. Phys. Chem. A* **1998**, *102*, 2572−2578.
(74) Cheng, Y.; Yang, S.; Hsu, C. Synthesis of Conjugated Polymers for Organic Solar Cell Applications. *Chem. Rev.* **2009**, *109*, 5868−5923.
(75) Carsten, B.; Szarko, J. M.; Son, H. J.; Wang, W.; Lu, L.; He, F.; Rolczynski, B. S.; Lou, S. J.; Chen, L. X.; Yu, L. Examining the Effect of the Dipole Moment on Charge Separation in Donor−Acceptor Polymers for Organic Photovoltaic Applications. *J. Am. Chem. Soc.* **2011**, *133*, 20468−20475.
(76) Salzner, U. Effect of Donor-Acceptor Substitution on Optoelectronic Properties of Conducting Organic Polymers. *J. Chem. Theory Comput.* **2014**, *10*, 4921−4937.
(77) Padmanabhan, J.; Parthasarathi, R.; Subramanian, V.; Chattaraj, P. K. Electrophilicity-Based Charge Transfer Descriptor. *J. Phys. Chem. A* **2007**, *111*, 1358−1361.
(78) Bultinck, P.; Fias, S.; Van Alsenoy, C.; Ayers, P. W.; Carbó-Dorca, R. Critical Thoughts on Computing Atom Condensed Fukui Functions. *J. Chem. Phys.* **2007**, *127*, 034102.
(79) Csonka, G. I.; Angyan, J. G. The Origin of the Problems with the PM3 Core Repulsion Function. *J. Mol. Struct.: THEOCHEM* **1997**, *93*, 31−38.
(80) IUPAC. *Compendium of Chemical Terminology*, 2nd ed. (the "Gold Book"). Compiled by McNaught, A. D.; Wilkinson, A.; Blackwell Scientific Publications: Oxford, U.K., 1997. XML on-line corrected version: http://goldbook.iupac.org (2006−) created by Nic, M.; Jirat, J.; Kosata, B.; updates compiled by A. Jenkins. ISBN 0-9678550-9-8. doi: 10.1351/goldbook.
(81) Pakiari, A. H.; Fakhraee, S. J. Electron Density Analysis of Weak van der Waals Complexess. *J. Theor. Comput. Chem.* **2006**, *5*, 621−631.
(82) Reed, A. E.; Curtiss, L. A.; Weinhold, F. Intermolecular Interactions from a Natural Bond Orbital, Donor-Acceptor Viewpoint. *Chem. Rev.* **1988**, *88*, 899−926.
(83) Buckingham, A. D.; Fowler, P. W.; Hutson, J. M. Theoretical Studies of van der Waals Molecules and Intermolecular Forces. *Chem. Rev.* **1988**, *88*, 963−988.
(84) Piacenza, M.; Grimme, S. Van der Waals Complexes of Polar Aromatic Molecules: Unexpected Structures for Dimers of Azulene. *J. Am. Chem. Soc.* **2005**, *127*, 14841−14848.
(85) Rohrer, J. Stacking and Band Structure of van der Waals Bonded Graphane Multilayers. *Phys. Rev. B: Condens. Matter Mater. Phys.* **2011**, *83*, 165423.
(86) Brochier Salon, M.-C.; Bayle, P.-A.; Abdelmouleh, M.; Boufi, S.; Naceur Belgacem, M. Kinetics of Hydrolysis and Self Condensation Reactions of Silanes by NMR Spectroscopy. *Colloids Surf., A* **2008**, *312*, 83−91.
(87) Abraham, R. J.; Byrne, J. J.; Griffiths, L.; Perez, M. 1H Chemical Shifts in NMR: Part 23. The Effect of Dimethyl Sulfoxide versus Chloroform Solvent on 1H chemical shifts. *Magn. Reson. Chem.* **2006**, *44*, 491−509.
(88) Kalinowski, H. O.; Berger, S.; Braun, S. *Carbon-13 NMR Spectroscopy*; Wiley J. & Sons Ltd.: New York, 1988.

DOI: 10.1021/acs.jpca.5b04167
J. Phys. Chem. A 2015, 119, 7038−7051